How to cite: *Angew. Chem. Int. Ed.* **2023**, *62*, e202305651
doi.org/10.1002/anie.202305651

Heterogeneous Catalysis | Hot Paper

Highly Efficient Decomposition of Perfluorocarbons for over 1000 Hours via Active Site Regeneration

Hang Zhang, Tao Luo, Yingkang Chen, Kang Liu, Hongmei Li, Evangelina Pensa, Junwei Fu, Zhang Lin, Liyuan Chai, Emiliano Cortés, and Min Liu**

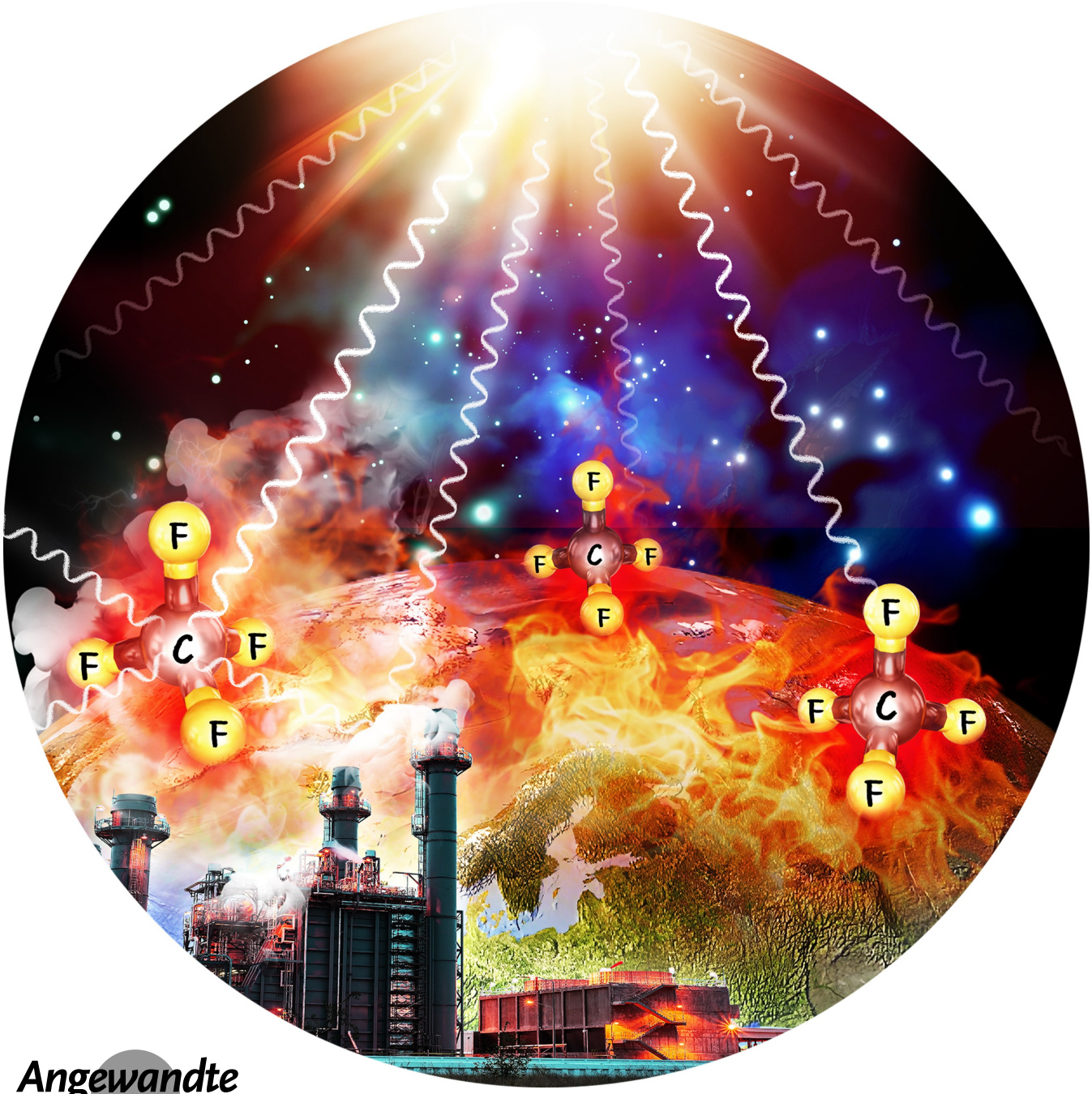

Angewandte International Edition Chemie

Abstract: Tetrafluoromethane (CF_4), the simplest perfluorocarbon (PFC), has the potential to exacerbate global warming. Catalytic hydrolysis is a viable method to degrade CF_4, but fluorine poisoning severely restricts both the catalytic performance and catalyst lifetime. In this study, Ga is introduced to effectively assists the defluorination of poisoned Al active sites, leading to highly efficient CF_4 decomposition at 600 °C with a catalytic lifetime exceeding 1,000 hours. ^{27}Al and ^{71}Ga magic-angle spinning nuclear magnetic resonance spectroscopy (MAS NMR) showed that the introduced Ga exists as tetracoordinated Ga sites (Ga_{IV}), which readily dissociate water to form Ga–OH. In situ diffuse reflectance infrared Fourier transform spectroscopy (DRIFTS) and density function theory (DFT) calculations confirmed that Ga–OH assists the defluorination of poisoned Al active sites via a dehydration-like process. As a result, the Ga/Al_2O_3 catalyst achieved 100 % CF_4 decomposition keeping an ultra-long catalytic lifetime and outperforming reported results. This work proposes a new approach for efficient and long-term CF_4 decomposition by promoting the regeneration of active sites.

Introduction

Perfluorocarbons (PFCs) have been listed among the most potent greenhouse gases—about 4 orders of magnitude higher than CO_2—with a very long atmospheric lifetime (3,000–50,000 years), according to the United Nations Framework Convention on Climate Change (UNFCCC, 2009).[1] Tetrafluoromethane (CF_4), the simplest PFCs, is one of the most abundant and harmful PFCs, owing to its high global warming potential (GWP) of 7,390 and long lifetime of 50,000 years.[2] Unfortunately, CF_4 has a perfectly symmetrical C–F bond with a strong bond energy of $543 \pm 4\ kJ\ mol^{-1}$, making it very hard to decompose.[3] Catalytic hydrolysis has been considered as the most effective technology for CF_4 decomposition due to its high decomposition rate at mild conditions and less harmful chemicals involved.[4] However, no report could achieve efficient decomposition of CF_4 for over 100 h at temperatures lower than 700 °C, owing to serious fluorine poisoning of the catalysts.[5]

The most efficient alumina-based catalysts have been found to be prone to F absorption on the Al active site, limiting the regeneration of Al active sites and seriously restricting the activity and stability of Al_2O_3.[4b,6] It has been reported that surface hydroxyl groups can assist in the defluorination of M–F (M = metal sites) through a dehydration-like reaction (M–OH + M–F → M–O–M + HF).[7] Vimont et al. reported that –OH facilitated the defluorination of Al–F over aluminum fluorides.[8] Francke et al. discovered that adjacent –OH promoted the defluorination of Cr–F by the creation of oxo M–O–Cr bridges.[9] Therefore, introduction of M–OH would be a promising way to assist in the defluorination of Al–F during CF_4 hydrolysis.

Herein, we developed a highly efficient decomposition method for CF_4 using Ga-doped Al_2O_3 (Ga/Al_2O_3), a highly stable catalyst which facilitates the active site regeneration. In situ diffuse reflectance infrared Fourier transform spectroscopy (DRIFTS) revealed that the hydrolysis-induced regeneration process of Al–F groups back to Al–OH over Al_2O_3 was slow, resulting in a poor catalyst activity and stability. However, the introduction of Ga–OH via Ga doping, accelerated the regeneration of the active Al–OH site by assisting the defluorination of Al–F. Consequently, the optimal 30 %Ga/Al_2O_3 catalyst, achieved 100 % CF_4 decomposition at 600 °C—which is among the lowest reported temperatures for this reaction—with an ultra-long catalytic lifetime of over 1000 h. This work proposes a novel mechanism for fluorine poisoning and regeneration of the catalytic active sites, providing an innovative pathway for efficient CF_4 decomposition using a highly stable catalyst.

Results and Discussion

The catalytic hydrolysis of CF_4 was evaluated over various catalysts with water (Figure 1). From 500 °C to 600 °C, $Ga/\theta\text{-}Al_2O_3$ catalyst consistently showed the highest CF_4 decomposition rate compared to $\gamma\text{-}Al_2O_3$ and $\theta\text{-}Al_2O_3$ (Figure 1a, S1 and S2). In particular, $Ga/\theta\text{-}Al_2O_3$ achieved 100 % CF_4 decomposition at even the low temperature of 600 °C, whereas only 81 % and 75 % were achieved for $\theta\text{-}Al_2O_3$ and $\gamma\text{-}Al_2O_3$, respectively. The CF_4 decomposition on a series of $Ga/\theta\text{-}Al_2O_3$ catalysts presented an initial

[*] H. Zhang, T. Luo, Y. Chen, Dr. K. Liu, H. Li, Prof. J. Fu, Prof. M. Liu
Hunan Joint International Research Center for Carbon Dioxide Resource Utilization, School of Physics and Electronics, Central South University
Changsha 410083, Hunan (P. R. China)
E-mail: minliu@csu.edu.cn
Dr. K. Liu, Prof. Z. Lin, Prof. L. Chai
School of Metallurgy and Environment, Central South University
Changsha 410083, Hunan (P. R. China)
Dr. K. Liu, Prof. Z. Lin, Prof. L. Chai
Chinese National Engineering Research Center for Control & Treatment of Heavy Metal Pollution
Changsha 410083, Hunan (P. R. China)
H. Li
School of Materials Science and Engineering, Zhengzhou University
Zhengzhou 450002, Henan (P. R. China)
Dr. E. Pensa, Prof. E. Cortés
Nanoinstitut München, Fakultät für Physik, Ludwig-Maximilians-Universität München
80539 München (Germany)
E-mail: Emiliano.Cortes@lmu.de

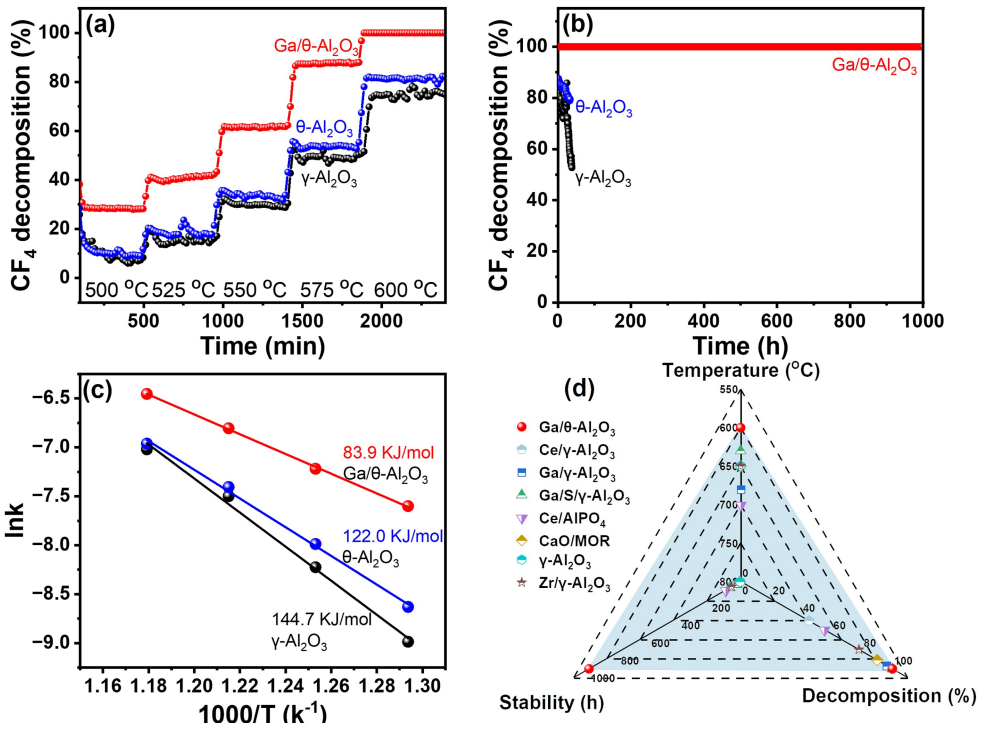

Figure 1. Catalytic stability and performance characterizations. (a) CF_4 decomposition (%) during CF_4 catalytic hydrolysis reaction at different reaction temperatures for γ-Al_2O_3 (black), θ-Al_2O_3 (blue) and Ga/θ-Al_2O_3 (red) catalysts (Reaction condition: 0.4 mL min^{-1} CF_4 in 32.9 mL min^{-1} Ar balance and 0.006 (liquid) or 8.16 (vapor) mL min^{-1} of water under atmospheric pressure, gas hourly space velocity (GHSV) = 1000 h^{-1}). (b) Stability test under 600 °C for the three catalysts under the same conditions: γ-Al_2O_3 (black), θ-Al_2O_3 (blue) and Ga/θ-Al_2O_3 (red). (c) Arrhenius plots obtained for the CF_4 decomposition rates at 500–575 °C for the three catalysts. (d) Comprehensive comparison of the activity parameters with the reported results.

increase with Ga doping, reaching a peak at 30 % Ga (Figure S3). Further increasing Ga content resulted in a significant decrease in the CF_4 decomposition rate, with 100 % Ga of Ga_2O_3 becoming inactive. Under 600 °C, γ-Al_2O_3 and θ-Al_2O_3 not only failed to achieve 100 % CF_4 decomposition but also lost approximately 40 % and 15 % of their activities, respectively, within a short period of 40 hours. Notably, no significant activity decline occurred on Ga/θ-Al_2O_3 for over 1,000 hours under the same conditions (Figure 1b).

To investigate intrinsic activity, the Arrhenius plots of catalysts for CF_4 decomposition from 500–575 °C were analyzed (Figure 1c). The apparent activation energy for Ga/θ-Al_2O_3 was only 83.9 kJ mol^{-1}, significantly lower than those of γ-Al_2O_3 (144.7 kJ mol^{-1}) and θ-Al_2O_3 (122.0 kJ mol^{-1}), demonstrating that Ga/θ-Al_2O_3 has the highest catalytic activity. A comprehensive comparison with reported CF_4 decomposition results (including alumina, aluminum phosphate and zeolite, Figure 1d and Table S1) reveals that the obtained Ga/θ-Al_2O_3 exhibited the lowest temperature for 100 % CF_4 decomposition, coupled with the longest catalytic lifetime, thus demonstrating its promising practical application.[6,10]

To investigate the morphology and physicochemical properties of the catalysts, we utilized several characterization methods which will be discussed below. Firstly, we performed X-ray diffraction (XRD). The XRD patterns of the Ga/θ-Al_2O_3 catalysts (Figure 2a) demonstrated that all samples could be assigned to θ-Al_2O_3 (JCPDS#35-0121) and no Ga_2O_3 feature was observed. Notably, the peak at 67° shifted negatively to a smaller angle as the Ga content increased, indicating successful doping of Ga into the catalysts. We determined the Ga contents by inductively coupled plasma mass spectrometry (ICP-MS), and the results are presented in Table S2. The actual Ga contents were found to be 8.4 %, 28.6 %, and 56.3 % for 10 %Ga/θ-Al_2O_3, 30 %Ga/θ-Al_2O_3, and 50 %Ga/θ-Al_2O_3 samples, respectively. These results suggest that Ga was almost fully doped into θ-Al_2O_3.

Transmission electron microscopy (TEM) was used to investigate the morphologies of the catalysts. The results revealed that the obtained θ-Al_2O_3 has a nanosheet structure with a thickness of only several nanometers and a width of tens of nanometers. Additionally, the introduction of Ga did not alter its nanosheet structure (see Figure S5). High resolution-TEM (HR-TEM) images showed that the lattice spacing distance changed from 1.96 Å to 2.03 Å with Ga doping, indicating successful doping of Ga into the Al_2O_3. Energy dispersive X-ray (EDX) mapping revealed that Ga is evenly distributed in Ga/θ-Al_2O_3 (Figure 2b), demonstrating the uniform distribution of Ga in Al_2O_3. To detect the local structure of Ga, ^{27}Al and ^{71}Ga magic-angle spinning nuclear magnetic resonance spectroscopies (MAS NMR) were performed (Figure 2c and 2d). The results

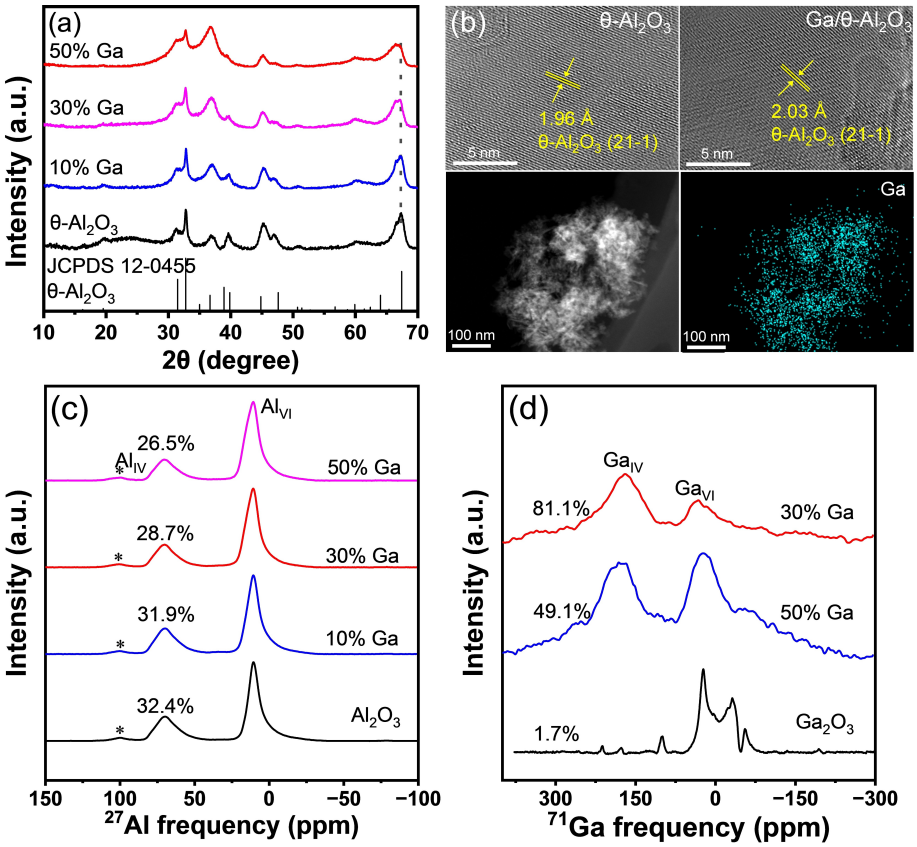

Figure 2. Structural characterization of the catalysts. (a) XRD patterns of the θ-Al_2O_3 and a series of Ga/θ-Al_2O_3 catalysts, (b) Top: HRTEM images of θ-Al_2O_3 and Ga/θ-Al_2O_3. Bottom: EDX mapping of Ga/θ-Al_2O_3. (c) and (d) ^{27}Al and ^{71}Ga MAS NMR spectra of samples, respectively. A sideband from a satellite transition signal is marked as asterisk.

showed that the tetracoordinated Al sites (Al_{IV}) decreased with the increase of tetracoordinated Ga sites (Ga_{IV}) in Ga/θ-Al_2O_3, demonstrating that the introduced Ga is predominantly in Ga_{IV} sites and facilitates the dissociation of water to produce Ga–OH.[11] Briefly, the ^{27}Al MAS NMR features at 11, 35 and 70 ppm in Figure 2c represent Al^{3+} ions in octahedral (Al_{VI}), pentahedron (Al_V) and tetrahedral (Al_{IV}) coordination, respectively. The content of Al decreased with Ga increasing, resulting in larger quadrupole interactions of Al and a slight broadening of the Al_{VI} peak. The broadening of the Al_{VI} peak will not affect the proportion of Al_{IV} (11 ppm) and Al_{VI} (70 ppm) sites. Moreover, the signal at ca. 100 ppm is associated with a sideband from a satellite transition signal (marked with an asterisk).

The specific surface area and the CF_4 adsorption capacity of the catalysts were tested to further evaluate their performance. The specific surface area of the catalysts decreased monotonically from 158.8 m^2g^{-1} to 97.7 m^2g^{-1} with increasing Ga doping (see Table S3), which rules out the possible effect of surface area. The temperature programmed desorption of CF_4 (CF_4-TPD) showed that the CF_4 adsorption capacities of γ-Al_2O_3 and θ-Al_2O_3 were higher than that of Ga/θ-Al_2O_3 (see Figure S8), indicating that the introduction of Ga did not improve the CF_4 adsorption capacity.

To explore the reaction mechanisms, catalytic reactions were performed using only CF_4, only H_2O, and CF_4 followed by H_2O, respectively. XRD and X-ray photoelectron spectroscopy (XPS) analyses showed clear diffraction peaks of AlF_3 and Al–F bonds on all γ-Al_2O_3, θ-Al_2O_3, and Ga/θ-Al_2O_3 samples treated with only CF_4 (Figures S9–S11), revealing the fluorine species generated on the catalysts.

Next, the dissociation of H_2O was carried out on Al_2O_3 samples and investigated by in situ DRIFTS. The results showed bands at 3500 cm^{-1}, 3691 cm^{-1}, and 3726 cm^{-1} for the hydroxyl of adsorbed water and Al–OH on catalysts (Figures 3a, 3b, S12, and S13). Notably, a new band at 3768 cm^{-1} was observed on both Ga/θ-Al_2O_3 and Ga_2O_3 (Figure S12), which could be attributed to Ga–OH. To analyze the effect of Ga on OH generation, the accumulation of OH signals from adsorbed water and catalyst surfaces over time was performed (Figures 3c and 3d). The results showed that the OH signal for adsorbed water increased faster than that of Al–OH on θ-Al_2O_3, indicating that the dissociation of H_2O on θ-Al_2O_3 is sluggish. In contrast, the opposite trend was observed on Ga/θ-Al_2O_3, with a faster growth of Al–OH, demonstrating that the introduced Ga promoted the generation of Al–OH.

To shed light on the crucial role of Ga doping in the defluorination of Al–F, we performed in situ DRIFTS

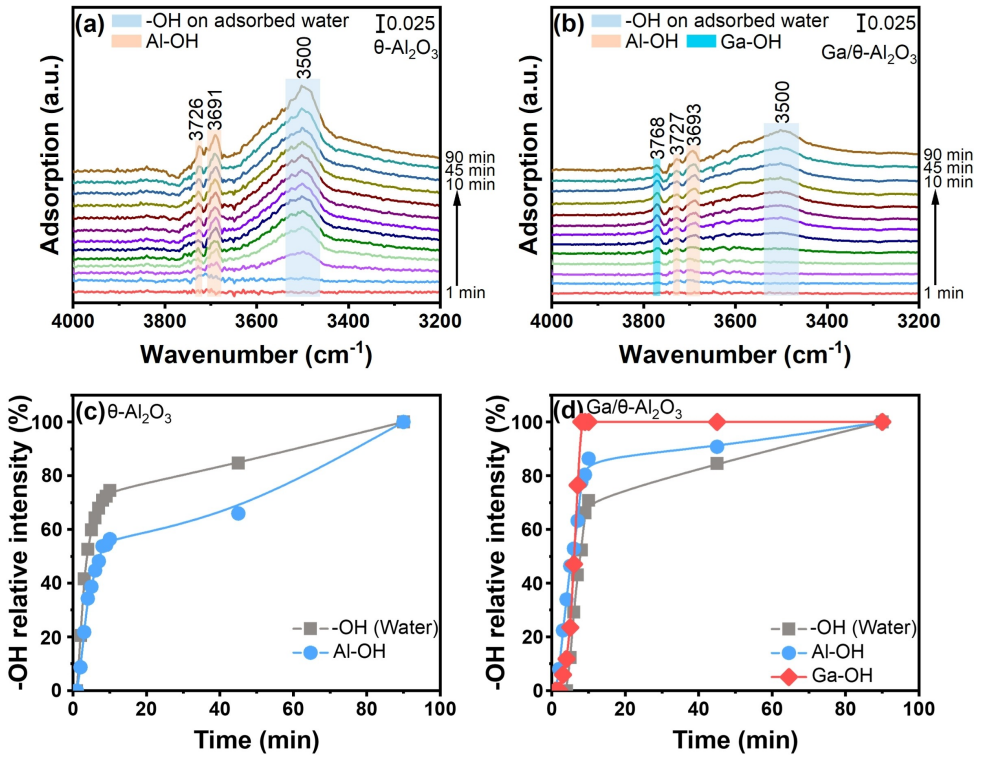

Figure 3. In situ DRIFTS of H_2O dissociation. (a and b) H_2O dissociation on θ-Al_2O_3 and Ga/θ-Al_2O_3 catalysts as a function of time Prior to the H_2O dissociation test, each sample was pretreated at 600 °C for 120 min under a 20 mL min^{-1} Ar flow. The background spectrum was collected after pretreatment at 600 °C. Then, a flow of water vapor was injected into the sample chamber via a deionized water bottle with Ar flow. The evolution of H_2O dissociation with time was recorded at 600 °C. (c and d) Evolution of hydroxyl bands (–OH) of adsorbed water and Ga/Al–OH over θ-Al_2O_3 and Ga/θ-Al_2O_3 catalysts, respectively.

experiments on θ-Al_2O_3 and Ga/θ-Al_2O_3 catalysts, exposing them first to CF_4 and then to H_2O addition (Figure 4). The increasing consumption of –OH represents the poisoning of the Al–OH active site, and the decreasing consumption of –OH represents the regeneration of the Al–OH active site. Our observations revealed that upon exposure to CF_4 both catalysts exhibited a rapid consumption of their hydrolyzed sites, i.e. Al–OH and Ga–OH sites, indicating significant poisoning of the active sites (Figures 4b and 4d). However, when we switched to H_2O addition, a remarkable difference between the two catalysts emerged: while only ≈23 % of the Al–OH sites were regenerated for θ-Al_2O_3, ≈61 % of the Al–OH sites were quickly restored for Ga/θ-Al_2O_3. This compelling finding demonstrates that Ga effectively assisted the defluorination of poisoned Al active sites. Additionally, 10 %Ga/θ-Al_2O_3 and 50 %Ga/θ-Al_2O_3 also showed feasible regeneration of the active site (Figure S15). These results demonstrated that Ga promoted the defluorination of Al–F and active site regeneration. Furthermore, density functional theory (DFT) calculations were carried out to investigate the reaction process. The results demonstrated the adsorption energy and bond length of hydroxyl and fluorine on θ-Al_2O_3 are −1.36 eV and −1.50 eV, and 1.95 Å and 1.87 Å, respectively (Figure S16). This suggests that Al has a stronger adsorption capacity for F compared to Ga. The low fluorine adsorption energy of −1.21 eV on the Ga site (Figure S17), and crystal orbital Hamilton population (COHP) between the Al/Ga center and the fluorine adatom (Figure S18), revealed weaker adsorption of F on Ga. These results demonstrated that it is feasible to assist the defluorination of poisoned Al active sites via introducing Ga sites. Based on these findings, a new mechanism of Ga assisting the defluorination of Al–F over Ga/θ-Al_2O_3 has been proposed in Figure 5. Initially, Al–OH reacts with CF_4 and forms inactive Al–F, which leads to fluorine poisoning on the Al active sites. Since F strongly adsorbs at the Al active site, it is challenging to regenerate from Al–F to Al–OH. However, Ga exhibits weaker adsorption of F, allowing Ga–F to easily hydrolyze into Ga–OH, thereby assisting the defluorination of poisoned Al active sites through a dehydration-like process. As a result, highly efficient CF_4 decomposition over a highly stable Ga/θ-Al_2O_3 catalyst was achieved by promoting active site regeneration.

Conclusion

In summary, Ga effectively assists in the defluorination of poisoned Al active sites over Ga/Al_2O_3, as demonstrated in this study. The optimized-composition of the Ga/Al_2O_3 catalyst—consisting of 30 % of Ga—delivered 100 % CF_4 decomposition with an ultra-long catalytic lifetime of over 1,000 h at 600 °C. Structural characterizations demonstrate

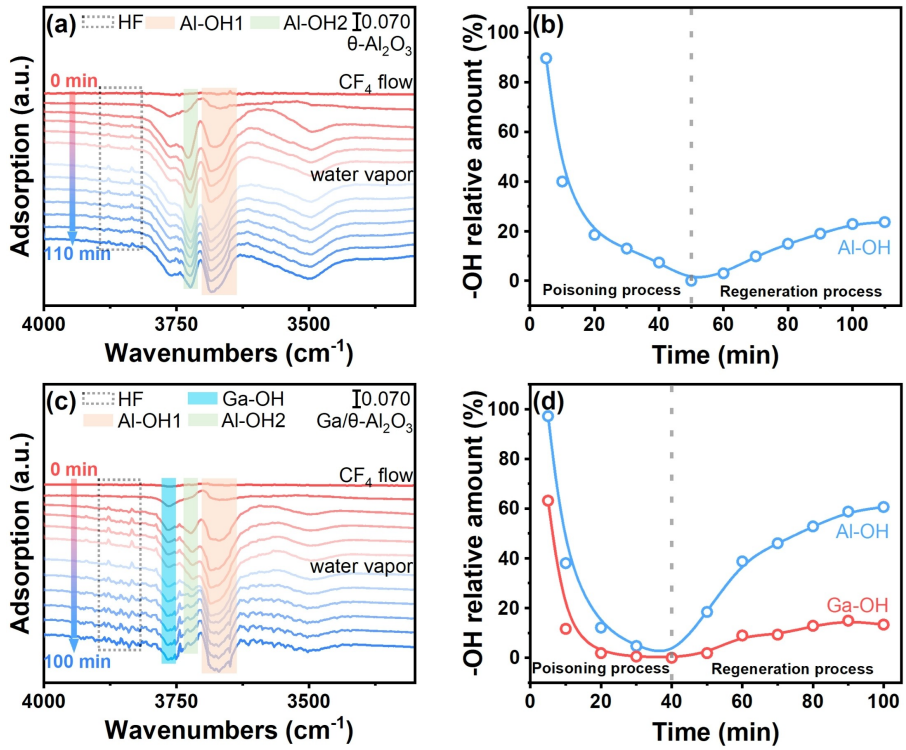

Figure 4. In situ DRIFTS of the CF_4 catalytic hydrolysis. (a and c) In situ DRIFTS over (a) θ-Al_2O_3 and (c) Ga/θ-Al_2O_3 catalysts with first only CF_4 followed with only H_2O. (b and d) Ga/Al–OH relative intensity on (b) θ-Al_2O_3 and (d) Ga/θ-Al_2O_3 catalysts as a function as time. Prior to the CF_4 catalytic hydrolysis test, each sample was pretreated at 600 °C for 120 min under a 20 mL min^{-1} Ar flow. The background spectrum was collected after pretreatment at 600 °C. Then, a 20 mL min^{-1} flow rate of 2500 ppm CF_4 was injected into the sample chamber with Ar balance, and the evolution of the CF_4 catalytic hydrolysis was recorded at 600 °C. One hour later, a flow of water vapor was injected into the sample chamber via a deionized water bottle with Ar flow. Meanwhile, the active site regeneration process was recorded as a function of time.

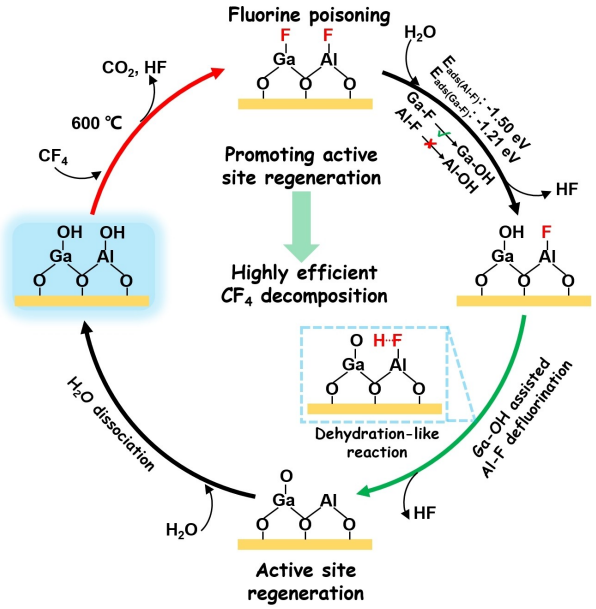

Figure 5. Schematic diagram. A new mechanism of Ga assisting the defluorination of Al–F over Ga/θ-Al_2O_3.

that Ga is introduced as Ga_{IV} site, facilitating the dissociation of water to produce Ga–OH. DFT calculations demonstrate that Ga–F is weaker than Al–F. In situ DRIFTS proved that Ga noticeably promoted the defluorination of Al–F through a dehydration-like process. This work presents a new approach for efficient decomposition of CF_4 for practical applications.

Acknowledgements

The authors acknowledge the support and funding from the National Natural Science Foundation of China (Grant Nos. 22376222 and 22002189), the Central South University Research Program of Advanced Interdisciplinary Studies (Grant No. 2023QYJC012), the Central South University Innovation-Driven Research Program (Grant No. 2023CXQD042), the Deutsche Forschungsgemeinschaft (DFG, German Research Foundation) under e-conversion Germany's Excellence Strategy—EXC 2089/1-390776260, the Bavarian program Solar Energies Go Hybrid (SolTech), the Center for NanoScience (CeNS) and the European Commission through the ERC Starting Grant CATALIGHT (802989). We are also grateful for resources from the High Performance Computing Center of Central South University. Open Access funding enabled and organized by Projekt DEAL.

Conflict of Interest

The authors declare no conflict of interest.

Data Availability Statement

The data that support the findings of this study are available from the corresponding author upon reasonable request.

Keywords: Active Site Regeneration · CF_4 · Gallium Doping · in-Situ DRIFTS

[1] a) L. Hockstad, L. Hanel, Inventory of US greenhouse gas emissions and sinks, **(2018)**, United States Environmental Protection Agency; b) K. Protocol, **1997**, Kyoto Protocol, UNFCCC Website, Available online: http://unfccc. int/kyoto_ protocol/items/2830. php (accessed on 1 January 2011); c) S. M. Wang, X. T. Mu, H. R. Liu, S. T. Zheng, Q. Y. Yang, *Angew. Chem. Int. Ed.* **2022**, *61*, e202207066; d) A. Taponard, T. Jarrosson, L. Khrouz, M. Médebielle, J. Broggi, A. Tlili, *Angew. Chem. Int. Ed.* **2022**, *61*, e202204623; e) L. Zámostná, T. Braun, B. Braun, *Angew. Chem. Int. Ed.* **2014**, *53*, 2745–2749.

[2] a) J. Harnisch, R. Borchers, P. Fabian, H. Gäggeler, U. Schotterer, *Nature* **1996**, *384*, 32; b) J. Marks, P. Nunez, in *Light Metals 2018* (Ed.: O. Martin), Springer, Cham, **2018**, pp. 1519–1525; c) J. Mühle, A. L. Ganesan, B. R. Miller, P. Salameh, C. Harth, B. Greally, M. Rigby, L. Porter, L. Steele, C. Trudinger, *Atmos. Chem. Phys.* **2010**, *10*, 5145–5164; d) V. Ramanathan, Y. Feng, *Atmos. Environ.* **2009**, *43*, 37–50; e) D. R. Worton, W. T. Sturges, L. K. Gohar, K. P. Shine, P. Martinerie, D. E. Oram, S. P. Humphrey, P. Begley, L. Gunn, J.-M. J. E. Barnola, *Environ. Sci. Technol.* **2007**, *41*, 2184–2189; f) W. Caminati, A. Maris, A. Dell'Erba, P. G. Favero, *Angew. Chem. Int. Ed.* **2006**, *45*, 6711–6714.

[3] a) L. Xia, X. J. Zeng, H. K. Li, B. Wu, S. X. J. A. C. Tian, *Angew. Chem. Int. Ed.* **2013**, *125*, 1047–1050; b) A. N. Ragan, Y. Kraemer, W. Y. Kong, S. Prasad, D. J. Tantillo, C. R. Pitts, *Angew. Chem. Int. Ed.* **2022**, *61*, e202208046.

[4] a) "The experimental study on high temperature air combustion and CF_4 decomposition": L. Jia, S. Ma, ASME Summer Heat Transfer Conference, **2005**, p. 47314; b) A. Anus, M. Sheraz, S. Jeong, E.-K. Kim, S. Kim, *J. Anal. Appl. Pyrolysis* **2021**, *156*, 105126; c) Y. S. Chen, K. L. Pan, A. Machmud, M. B. Chang, *Int. J. Plasma Environ. Sci. Technol.* **2021**, *15*, e03004; d) S. Jo, D. Cho, D. H. Lee, W. S. Kang, *Plasma Chem. Plasma Process.* **2022**, *42*, 1311–1327; e) J. Ko, T. Kim, S. Choi, *Plasma Sci. Technol.* **2019**, *21*, 064002; f) J. D. Krug, P. M. Lemieux, C.-W. Lee, J. V. Ryan, P. H. Kariher, E. P. Shields, L. C. Wickersham, M. K. Denison, K. A. Davis, D. A. Swensen, *J. Air Waste Manage. Assoc.* **2022**, *72*, 256–270; g) K. L. Pan, Y. S. Chen, M. B. Chang, *Plasma Chem. Plasma Process.* **2019**, *39*, 877–896; h) O. Živný, M. Hlína, A. Serov, A. Halinouski, A. Mašláni, *Plasma Chem. Plasma Process.* **2020**, *40*, 309–323.

[5] a) C.-K. Chen, A. Shiue, D.-W. Huang, C.-T. Chang, *J. Nanosci. Nanotechnol.* **2014**, *14*, 3202–3208; b) J. Y. Han, C. H. Kim, B. Lee, S. Jeong, H. Lim, K. Y. Lee, S. K. Ryi, *Greenhouse Gases Sci. Technol.* **2017**, *7*, 1141–1149; c) J.-Y. Han, C.-H. Kim, B. Lee, S.-C. Nam, H.-Y. Jung, H. Lim, K.-Y. Lee, S.-K. Ryi, *Front. Chem. Sci. Eng.* **2017**, *11*, 537–544.

[6] H. Zhang, T. Luo, Y. Long, Y. Chen, J. Fu, H. Liu, J. Hu, Z. Lin, L. Chai, M. J. E. S. N. Liu, *Environ. Sci.-Nano* **2022**, *9*, 954–963.

[7] a) D.-W. Cho, Y.-S. Han, J. Lee, J.-Y. Jang, G.-J. Yim, S. Cho, J.-S. Lee, Y.-W. Cheong, *Chemosphere* **2020**, *247*, 125899; b) J. Fan, K. Chen, J. Xu, A. Khaldun, Y. Chen, L. Chen, X. Yan, *Ecotoxicol. Environ. Saf.* **2022**, *231*, 113192; c) R. Liu, J. Ju, Z. He, C. Hu, H. Liu, J. Qu, *Colloids Surf. A* **2016**, *504*, 95–104; d) X. Liu, Y. Jiao, Y. Zheng, M. Jaroniec, S.-Z. Qiao, *J. Am. Chem. Soc.* **2019**, *141*, 9664–9672; e) S. Dubey, M. Agarwal, A. B. Gupta, *J. Mol. Liq.* **2018**, *266*, 349–360; f) B. Wang, H. Xu, D. Wang, S. J. C. He, S. A. Physicochemical, E. Aspects, *Colloids Surf. A* **2021**, *615*, 126124; g) K. Fan, Y. Wang, Y. Liu, Y. Li, Y. Chen, Y. Meng, X. Liu, W. Feng, X. Wang, *Adv. Mater. Interfaces* **2020**, *7*, 2000915.

[8] A. Vimont, J.-C. Lavalley, L. Francke, A. Demourgues, A. Tressaud, M. Daturi, *J. Phys. Chem. B* **2004**, *108*, 3246–3255.

[9] L. Francke, E. Durand, A. Demourgues, A. Vimont, M. Daturi, A. Tressaud, *J. Mater. Chem.* **2003**, *13*, 2330–2340.

[10] a) S. Araki, Y. Hayashi, S. Hirano, H. Yamamoto, *J. Environ. Chem. Eng.* **2020**, *8*, 103763; b) Z. El-Bahy, R. Ohnishi, M. Ichikawa, *Appl. Catal. B* **2003**, *40*, 81–91; c) Z. M. El-Bahy, R. Ohnishi, M. Ichikawa, *Catal. Today* **2004**, *90*, 283–290; d) J. Y. Jeon, X.-F. Xu, M. H. Choi, H. Y. Kim, Y.-K. Park, *Chem. Commun.* **2003**, 1244–1245; e) J.-Y. Song, S.-H. Chung, M.-S. Kim, M.-G. Seo, Y.-H. Lee, K.-Y. Lee, J.-S. Kim, *J. Mol. Catal. A* **2013**, *370*, 50–55; f) Y. Takita, C. Morita, M. Ninomiya, H. Wakamatsu, H. Nishiguchi, T. J. C. L. Ishihara, *Chem. Lett.* **1999**, *28*, 417–418; g) X.-F. Xu, J. Y. Jeon, M. H. Choi, H. Y. Kim, W. C. Choi, Y.-K. J. C. L. Park, *Chem. Lett.* **2005**, *34*, 364–365; h) X.-F. Xu, J. Y. Jeon, M. H. Choi, H. Y. Kim, W. C. Choi, Y.-K. J. J. O. M. C. A. C. Park, *J. Mol. Catal. A* **2007**, *266*, 131–138.

[11] a) P. Castro-Fernández, M. Kaushik, Z. Wang, D. Mance, E. Kountoupi, E. Willinger, P. M. Abdala, C. Copéret, A. Lesage, A. Fedorov, *Chem. Sci.* **2021**, *12*, 15273–15283; b) M. W. Schreiber, C. P. Plaisance, M. Baumgärtl, K. Reuter, A. Jentys, R. Bermejo-Deval, J. A. Lercher, *J. Am. Chem. Soc.* **2018**, *140*, 4849–4859; c) Y. Zhou, H. Thirumalai, S. K. Smith, K. H. Whitmire, J. Liu, A. I. Frenkel, L. C. Grabow, J. D. Rimer, *Angew. Chem. Int. Ed.* **2020**, *59*, 19592–19601; d) A. Friedrich, J. Eyselein, J. Langer, C. Färber, S. Harder, *Angew. Chem. Int. Ed.* **2021**, *60*, 16492–16499.

Manuscript received: April 22, 2023
Accepted manuscript online: August 23, 2023
Version of record online: September 4, 2023